BPX preconditioners for the Bidomain model of electrocardiology

D. Ottino[a], S. Scacchi[a]

[a] *Dipartimento di Matematica, Università degli Studi di Milano, Via Saldini 50, 20133 Milano, Italy. E-mail:* daniela.ottino@studenti.unimi.it, simone.scacchi@unimi.it.

Abstract

The aim of this work is to develop a BPX preconditioner for the Bidomain model of electrocardiology. This model describes the bioelectrical activity of the cardiac tissue and consists of a system of a non-linear parabolic reaction-diffusion partial differential equation (PDE) and an elliptic linear PDE, modeling at macroscopic level the evolution of the transmembrane and extracellular electric potentials of the anisotropic cardiac tissue. The evolution equation is coupled through the non-linear reaction term with a stiff system of ordinary differential equations, the so-called membrane model, describing the ionic currents through the cellular membrane. The discretization of the coupled system by finite elements in space and semi-implicit finite differences in time yields at each time step the solution of an ill-conditioned linear system. The goal of the present study is to construct, analyze and numerically test a BPX preconditioner for the linear system arising from the discretization of the Bidomain model. Optimal convergence rate estimates are established and verified by two- and three-dimensional numerical tests on both structured and unstructured meshes. Moreover, in a full heartbeat simulation on a three-dimensional wedge of ventricular tissue, the BPX preconditioner is about 35% faster in terms of CPU times than ILU(0) and an Algebraic Multigrid preconditioner.

Keywords: BPX preconditioner, Bidomain model, reaction-diffusion system

1. Introduction

The Bidomain model describes the bioelectrical activity of the cardiac tissue and is constituted by a non-linear parabolic reaction-diffusion partial differential equation (PDE) and an elliptic linear PDE. This system models at macroscopic level the evolution of the transmembrane and extracellular electric potentials, v and u_e respectively, of the anisotropic cardiac tissue (macroscale). The evolution equation is coupled through the non-linear reaction term with a stiff system of ordinary differential equations (ODEs), the so-called membrane model, describing the ionic currents flowing through the cellular membrane (microscale).

The different space and time scales involved make the solution of the Bidomain system a very challenging problem in the field of scientific computing. In fact, the accurate approximation of the steep activation wavefront spreading through the cardiac tissue during the excitation phase requires mesh sizes on the order of the tenth of millimeter and time step sizes on the order of the hundredth of millisecond, while the dimension of the heart muscle is on the order of centimeters and the duration of heartbeat on the order of seconds. Thus, the discretization of the anisotropic Bidomain model in three-dimensional ventricular geometries of realistic size yields the solution of large scale (often exceeding $O(10^6)$ unknowns) and ill-conditioned linear systems at each time step.

Several approaches have been developed in order to reduce the high computational costs of the Bidomain model. Fully implicit methods in time, requiring the solution of non-linear systems at each time step, have been considered in the literature, see e.g. [1, 2, 3, 4]. Alternatively, most previous works have considered semi-implicit (IMEX) time discretizations and/or operator splitting schemes, where the reaction and diffusion terms are treated separately, see e.g. [5, 6, 7, 8, 9, 10, 11, 12, 13, 14, 15]. The advantage of IMEX and operator splitting schemes is that they only require the solution of linear systems at each time step. Many different preconditioners have been proposed in order to devise efficient iterative solvers for such linear systems: SSOR [16], block diagonal or triangular [17, 18, 19, 20, 21, 22, 23], optimized Schwarz [24, 25], geometric multigrid [26, 27], algebraic multigrid [28, 17, 29, 18, 19], multilevel Schwarz [30, 31, 32], Neumann-Neumann and BDDC [33, 34] preconditioners.

The Bramble-Pasciak-Xu (BPX) preconditioner is a multilevel method introduced in [35] for the solution of linear systems arising from the finite element discretization of elliptic problems. This preconditioner has been proved to be particularly effective in case of local refinement, see [36, 37, 38]. In the last years, space adaptivity has been largely employed to reduce the high computational costs required by the solution of the Bidomain model, see e.g. [39, 40, 41, 42, 43, 44, 45].

In order to build a Bidomain preconditioner effective in case of local refinement, the aim of this work is to construct, analyze and test numerically the BPX preconditioner for the Bidomain model. Optimal convergence rate estimates have been established by applying the abstract BPX theory of [35, 38] to the Bidomain bilinear form. Several numerical tests on two- and three-dimensional structured and unstructured meshes have confirmed the theoretical results. The numerical tests have also shown that, in a full heartbeat simulation on a three-dimensional wedge of ventricular tissue, the BPX preconditioner is about 35% faster in terms of CPU times than ILU(0) and Algebraic Multigrid preconditioners.

The paper is organized as follows. In Section 2 and 3, we present the Bidomain model and its discretization. In Section 4, we recall the abstract theory of the BPX preconditioner and we construct and analyze the BPX preconditioner applied to the Bidomain system. Finally, the results of several numerical tests are reported in Section 5.

2. The Bidomain model

2.1. The macroscopic Bidomain model

The heart is a pump, which by contracting and expanding drives the blood around the body. Coordination of the mechanical activity is provided by an electric signal. At a microscopic level, the heart is composed of elongated cells, surrounded by the extracellular space and connected to each other through special electrical junctions, called *gap junctions*, see [46, 47].

From a microscopic model of the discrete cellular structure, it is possible to derive, by a homogenization process a macroscopic model, see [48]. In this model, called macroscopic Bidomain model, the cardiac tissue is described as the superposition of two anisotropic continuous media, the intra- and extracellular media, which coexist at every point of the tissue and are connected by a cellular membrane, distributed in a continuous way, see [49]. The intracellular domain represents the region internal to the cells, while the extracellular domain represents the space around cells. A third region may be included to represent the extramyocardial domain. This region can be used to model a fluid bath in experimental conditions or the torso. In the following we consider the insulated Bidomain model, with only the intra- and the extracellular domains, see [50].

Since in the homogenized representation of the Bidomain model the cardiac domain coincides with the superposition of the intra- (i) and extra- (e) cellular domains, we have

$\Omega \equiv \Omega_i \equiv \Omega_e \subset \mathbb{R}^3$ is the physical region occupied by the heart,
u_i, $u_e : \Omega \to \mathbb{R}$ are the intra- ed extracellular electric potentials,
$v := u_i - u_e : \Omega \to \mathbb{R}$ is the transmembrane potential.

The anisotropic structure of the continuous media is characterized by the conductivity tensors D_i and D_e. The anisotropic conductivity is related to the arrangement of the cardiac fibers, whose direction rotates counterclockwise from the epicardium to the endocardium. The ventricular myocardium has a laminar structure composed of muscle sheets. In this organization, it is possible to identify three principal axes at any point $\mathbf{x}$. Let $\mathbf{a}_l(\mathbf{x})$, $\mathbf{a}_t(\mathbf{x})$, $\mathbf{a}_n(\mathbf{x})$ be a triplet of orthonormal vectors at a point $\mathbf{x}$, where $\mathbf{a}_l$ is parallel to the local fiber direction, $\mathbf{a}_t$ is tangent to the radial lamina, and $\mathbf{a}_n$ is normal to the muscle sheet, and the latter two are transversal to the fiber axis. Generally, this triplet depends on the position $\mathbf{x}$ in the myocardium. Let $\sigma_l^{i,e}$, $\sigma_t^{i,e}$, $\sigma_n^{i,e}$ be the conductivity coefficients of the intra- and extracellular media, measured along the corresponding directions $\mathbf{a}_l$, $\mathbf{a}_t$, $\mathbf{a}_n$. Generally, these coefficient may depend on $\mathbf{x}$, but in the following we assume that they are constant, i.e. a condition of homogenous anisotropy. Thus the anisotropic conductivity tensors D_i and D_e are given by:

$$D_{i,e}(\mathbf{x}) = \sigma_l^{i,e}\mathbf{a}_l(\mathbf{x})\mathbf{a}_l^T(\mathbf{x}) + \sigma_t^{i,e}\mathbf{a}_t(\mathbf{x})\mathbf{a}_t^T(\mathbf{x}) + \sigma_n^{i,e}\mathbf{a}_n(\mathbf{x})\mathbf{a}_n^T(\mathbf{x}). \tag{1}$$

The bioelectrical activity of the cardiac cells is due to the flow I_{ion} (per unit area of the membrane surface) of various ionic currents (among which the most important are sodium, potassium and calcium) through the cellular membrane. The cellular membrane behaves as a capacitor, so the total membrane current per unit volume i_m is given by

$$i_m = \chi\left(C_m\frac{\partial v}{\partial t} + I_{ion}\right),$$

where $v = u_i - u_e$ is the transmembrane potential, the coefficient χ is the ratio of membrane area per tissue volume, C_m is the membrane capacitance and I_{ion} is the sum of all ionic currents, dependent on the membrane model, see the Appendix.

In an insulated case, any current that leaves one domain must cross the cell membrane and flow into the other domain. This requires the change in current density in each of the domains to be equal in magnitude and opposite in sign and also to be equal to the current flow across the membrane. So we have $\operatorname{div}\mathbf{J}_i = -\operatorname{div}\mathbf{J}_e = i_m$, where $\mathbf{J}_{i,e} = -D_{i,e}\nabla u_{i,e}$ are the intra- ed extracellular current densities.

Therefore, in the Bidomain model the space-time evolution of the intra- and extracellular potentials u_i and u_e is modeled by the following reaction-diffusion system of PDEs, coupled with an ODEs system for N_w gating variables w and N_c ionic concentration variables c, with N_w and N_c dependent on the membrane model.

Given

$i_{app}^e : \Omega \times (0,T) \to \mathbb{R}$ extracellular applied current per unit volume,
$v_0 : \Omega \to \mathbb{R}$ initial condition for the transmembrane potential,
$w_0 : \Omega \to \mathbb{R}^{N_w}$ initial condition for the gating variables,

$c_0 : \Omega \to \mathbb{R}^{N_c}$ initial condition for the ionic concentrations variables,
find

u_i, $u_e : \Omega \times (0,T) \to \mathbb{R}$ intra- and extracellular potentials,
$v = u_i - u_e : \Omega \times (0,T) \to \mathbb{R}$ transmembrane potential,
$w : \Omega \times (0,T) \to \mathbb{R}^{N_w}$ gating variables,
$c : \Omega \times (0,T) \to \mathbb{R}^{N_c}$ ionic concentrations variables
such that

$$\begin{cases} c_m \dfrac{\partial v}{\partial t} - \operatorname{div}(D_i \nabla u_i) + i_{ion}(v,w,c) = 0 & \text{in } \Omega \times (0,T) \\ -c_m \dfrac{\partial v}{\partial t} - \operatorname{div}(D_e \nabla u_e) - i_{ion}(v,w,c) = i^e_{app} & \text{in } \Omega \times (0,T) \\ \dfrac{\partial w}{\partial t} - R(v,w) = 0, & \text{in } \Omega \times (0,T) \\ \dfrac{\partial c}{\partial t} - S(v,w,c) = 0, & \text{in } \Omega \times (0,T), \end{cases} \tag{2}$$

where $c_m = \chi C_m$ and $i_{ion} = \chi I_{ion}$.

We assume that the cardiac tissue is insulated, thus homogeneous Neumann boundary conditions are imposed on $\partial\Omega \times (0,T)$:

$$\mathbf{n}^T D_i \nabla u_i = 0, \quad \mathbf{n}^T D_e \nabla u_e = 0,$$

where $\mathbf{n}$ is the outward normal to $\partial\Omega$. Initial conditions are assigned on Ω at $t = 0$

$$v(\mathbf{x},0) = u_i(\mathbf{x},0) - u_e(\mathbf{x},0) = v_0(\mathbf{x}), \quad w(\mathbf{x},0) = w_0(\mathbf{x}).$$

The analytical expression of the functions I_{ion} in the reaction term and R in the right hand side of the ODEs depends on the membrane model chosen. In this paper, we consider the Luo-Rudy phase I (LR1) model, see [51].

Adding the two equations of the system (2), integrating on the domain Ω and applying the divergence theorem, from the Neumann boundary conditions we have the compatibility condition, necessary for the (2) to be solvable:

$$\int_\Omega i^e_{app}\, dx = 0.$$

The potentials u_i and u_e are determined up to the same time-dependent additive constant, while v is uniquely determined. The common constant is related to the reference potential, usually chosen such that u_e has zero average on Ω, i.e.

$$\int_\Omega u_e dx = 0.$$

System (2) can be equivalently rewritten in terms of the transmembrane and extracellular potentials $v(\mathbf{x},t)$ and $u_e(\mathbf{x},t)$, thus obtaining the parabolic-elliptic (PE) formulation of the Bidomain

model, considered in the rest of this paper:

$$\begin{cases} c_m \dfrac{\partial v}{\partial t} - \mathrm{div}(D_i \nabla v) - \mathrm{div}(D_i \nabla u_e) + i_{ion}(v,w,c) = 0 & \text{in } \Omega \times (0,T) \\ -\mathrm{div}(D_i \nabla v) - \mathrm{div}((D_i + D_e)\nabla u_e) = i^e_{app} & \text{in } \Omega \times (0,T) \\ \dfrac{\partial w}{\partial t} - R(v,w) = 0, & \text{in } \Omega \times (0,T) \\ \dfrac{\partial c}{\partial t} - S(v,w,c) = 0, & \text{in } \Omega \times (0,T) \\ \mathbf{n}^T D_i \nabla (v + u_e) = 0 & \text{in } \partial\Omega \times (0,T) \\ \mathbf{n}^T (D_i + D_e)\nabla u_e + \mathbf{n}^T D_i \nabla v = 0, & \text{in } \partial\Omega \times (0,T) \\ v(\mathbf{x},0) = v_0(\mathbf{x}), \quad w(\mathbf{x},0) = w_0(\mathbf{x}), \quad c(\mathbf{x},0) = c_0(\mathbf{x}) & \text{in } \Omega. \end{cases} \tag{3}$$

2.2. Variational formulation

Assume that

(H1) the cardiac region Ω is a bounded Lipschitz connected open subset of $\mathbb{R}^3$;

(H2) the tensors $D_{i,e}(\mathbf{x})$ satisfy the following uniform ellipticity condition:

$$\exists\, \alpha_{i,e}, C_{i,e} > 0 : \quad \alpha_{i,e}|\xi|^2 \le \xi^T D_{i,e}(\mathbf{x})\xi \le C_{i,e}|\xi|^2, \quad \forall \xi \in \mathbb{R}^3,\, \mathbf{x} \in \Omega;$$

(H3) the coefficients of $D_{i,e}(\mathbf{x})$ are Lipschitz continuous.

Let V be the Sobolev space $H^1(\Omega)$, define the spaces

$$\widetilde{V} = \{\psi \in V : \int_\Omega \psi = 0\} \qquad \text{and} \qquad U = V \times \widetilde{V} = \{u = (\varphi, \psi) : \varphi \in V, \psi \in \widetilde{V}\},$$

define the usual L^2-inner product $(\varphi, \psi) = \int_\Omega \varphi\psi dx \quad \forall \varphi, \psi \in L^2(\Omega)$, and the elliptic bilinear forms

$$\begin{aligned} a_{i,e}(\varphi, \psi) &= \int_\Omega (\nabla\varphi)^T D_{i,e}(x) \nabla\psi dx, \\ a(\varphi, \psi) &= \int_\Omega (\nabla\varphi)^T D(x) \nabla\psi dx \quad \forall \varphi, \psi \in H^1(\Omega), \end{aligned}$$

where $D = D_i + D_e$ is the bulk conductivity tensor.

The variational formulation of the Bidomain system (3) reads as follows. Given $v_0, w_0 \in L^2(\Omega)$, $i^e_{app} \in L^2(\Omega \times (0,T))$, find $v \in L^2(0,T;V)$, $u_e \in L^2(0,T;\widetilde{V})$, $w \in L^2(0,T;L^2(\Omega)^{N_w})$ and $c \in L^2(0,T;L^2(\Omega)^{N_c})$ such that $\dfrac{\partial v}{\partial t} \in L^2(0,T;V)$, $\dfrac{\partial w}{\partial t} \in L^2(0,T;L^2(\Omega)^{N_w})$, $\dfrac{\partial c}{\partial t} \in L^2(0,T;L^2(\Omega)^{N_c})$ and $\forall t \in (0,T)$

$$\begin{cases} c_m \dfrac{\partial}{\partial t}(v, \hat{v}) + a_i(v, \hat{v}) + a_i(u_e, \hat{v}) + (i_{ion}(v,w), \hat{v}) = 0 & \forall \hat{v} \in V \\ a_i(v, \hat{u}_e) + a(u_e, \hat{u}_e) = (i^e_{app}, \hat{u}_e) & \forall \hat{u}_e \in V \\ \dfrac{\partial}{\partial t}(w, \hat{w}) - (R(v,w), \hat{w}) = 0, & \forall \hat{w} \in L^2(\Omega)^{N_w} \\ \dfrac{\partial}{\partial t}(c, \hat{c}) - (S(v,w,c), \hat{c}) = 0, & \forall \hat{c} \in L^2(\Omega)^{N_c}, \end{cases} \tag{4}$$

with the appropriate initial conditions in (3). For the mathematical analysis of this model we refer to [52, 53].

3. Discretization and numerical methods

System (4) is discretized by the finite element method in space and a semi-implicit method in time.

Time discretization. The time discretization is performed by a semi-implicit method using for the diffusion term the implicit Euler method, while the non-linear reaction term i_{ion} is treated explicitly. The implicit treatment of the diffusion terms appearing in the Bidomain model is essential in order to adaptively change the time step according to the stiffness of the various phases of the heartbeat. The ODE system of the LR1 membrane model is discretized by the implicit Euler method for the gating variables ODEs and by the explicit Euler method for the ionic concentration ODE. As a consequence, the full evolution system (4) is decoupled by first solving the gating and ion concentrations system (given the transmembrane potential $v^n = u_i^n - u_e^n$ at the previous time-step)

$$\begin{cases} (w^{n+1} - \Delta t\, R(v^n, w^{n+1}), \hat{w}) = (w^n, \hat{w}) & \forall \hat{w} \in L^2(\Omega)^{N_w} \\ (c^{n+1}, \hat{c}) = (c^n + \Delta t\, S(v^n, w^{n+1}, c^n), \hat{c}) & \forall \hat{c} \in L^2(\Omega)^{N_c} \end{cases} \tag{5}$$

and then solving for $(v^{n+1}, u_e^{n+1}) \in U$ the PE variational problem

$$\begin{cases} c_t(v^{n+1}, \hat{v}) + a_i(v^{n+1}, \hat{v}) + a_i(u_e^{n+1}, \hat{v}) = (c_t\ v^n - i_{ion}(v^n, w^{n+1}, c^{n+1}), \hat{v}) & \forall \hat{v} \in V \\ a_i(v^{n+1}, \hat{u}_e) + a(u_e^{n+1}, \hat{u}_e) = (i_{app}^e, \hat{u}_e) & \forall \hat{u}_e \in V \end{cases} \tag{6}$$

where $c_t = \frac{c_m}{\Delta t}$.

Lemma 3.1. *The symmetric bilinear forms $((\cdot,\cdot))$, $((\cdot,\cdot))_0 : U \times U \to \mathbb{R}$ defined by*

$$\begin{aligned} ((u, \hat{u})) : &= \int_\Omega v\hat{v} + \int_\Omega \nabla v \cdot \nabla \hat{v} + \int_\Omega \nabla u_e \cdot \nabla \hat{u}_e \\ ((u, \hat{u}))_0 : &= \int_\Omega v\hat{v} + \int_\Omega u_e \hat{u}_e \end{aligned}$$

are inner products on U. Here $u = (v, u_e), \hat{u} = (\hat{v}, \hat{u}_e)$ in $((\cdot,\cdot))$.

We denote by $|||\cdot|||$, $|||\cdot|||_0 : U \to \mathbb{R}$ the norms induced by the $((\cdot,\cdot))$, $((\cdot,\cdot))_0$ inner products, i.e.

$$\begin{aligned} |||u|||^2 &= \int_\Omega v^2 + \int_\Omega |\nabla v|^2 + \int_\Omega |\nabla u_e|^2 \\ |||u|||_0^2 &= \int_\Omega v^2 + \int_\Omega u_e^2. \end{aligned}$$

Lemma 3.2. *The bilinear form $a_{bid}(\cdot,\cdot) : U \times U \to \mathbb{R}$ defined by*

$$a_{bid}(u, \hat{u}) : = c_t \int_\Omega v\hat{v} + \int_\Omega D_i \nabla(v + u_e) \cdot \nabla(\hat{v} + \hat{u}_e) + \int_\Omega D_e \nabla u_e \cdot \nabla \hat{u}_e,$$

is continuous and elliptic with respect to the $|||\cdot|||$ norm.

The stationary Bidomain system (6) can be rewritten in the compact form:
given v^n, w^{n+1}, find $u^{n+1} \in U$ such that

$$a_{bid}(u^{n+1}, \hat{u}) = (F_i, \hat{v}) + (F_e, \hat{u}_e) \quad \forall \hat{u} = (\hat{v}, \hat{u}_e) \in V \times V, \tag{7}$$

with $F_i = c_t\ v^n - i_{ion}(v^n, w^{n+1}, c^{n+1})$ and $F_e = i_{app}^e$.

Remark 3.1. *We note that, if (H1)-(H2)-(H3) hold, problem (7) is H^2-regular, i.e.*

$$|v|_{H^2(\Omega)} + |u_e|_{H^2(\Omega)} \quad \leq \quad C(||F_i||_{L^2(\Omega)} + ||F_e||_{L^2(\Omega)}). \tag{8}$$

Space discretization. The domain Ω is discretized by introducing a quasi-uniform triangulation $\mathcal{T}_h$, with mesh size denoted by h. Denote by V^h the associated finite element space. In this work, we will consider P_1 and Q_1 finite elements. Define also the spaces

$$\widetilde{V}^h = \{\psi^h \in V^h : \int_\Omega \psi^h = 0\} \quad \text{and} \quad U^h = V^h \times \widetilde{V}^h.$$

The discrete Bidomain system is obtained by applying a standard Galerkin procedure, yielding the same equations as in (6), with e.g. $v^{h,n}$ instead of v^n. Choose now a finite element basis $\{\varphi_i\}$ for V_h and let $\mathrm{M} = (\mathrm{m}_{rs})$, $\mathrm{A}_{i,e} = (\mathrm{a}^{i,e}_{rs})$ and $\mathrm{A} = (\mathrm{a}_{rs})$ be the symmetric mass and stiffness matrices defined by

$$\mathrm{m}_{rs} = \sum_E \int_E \varphi_r\, \varphi_s \mathrm{dx},$$
$$\mathrm{a}^{i,e}_{rs} = \sum_E \int_E (\nabla\varphi_r)^T D_{i,e}(\mathbf{x})\, \nabla\varphi_s \mathrm{dx}, \quad \mathrm{a}_{rs} = \sum_E \int_E (\nabla\varphi_r)^T D(\mathbf{x})\, \nabla\varphi_s \mathrm{dx}.$$

Numerical quadrature with a simple trapezoidal rule in three dimensions is used in order to compute these integrals. We can now write in matrix form the discrete formulation of (6).

Given $\mathbf{v}^n$, $\mathbf{w}^n$, $\mathbf{c}^n$, we first find $\mathbf{w}^{n+1}$, $\mathbf{c}^{n+1}$ by solving

$$\begin{cases} \mathbf{w}^{n+1} - \Delta t\, R(\mathbf{v}^n, \mathbf{w}^{n+1}) = \mathbf{w}^n \\ \mathbf{c}^{n+1} = \mathbf{c}^n + \Delta t\, S(\mathbf{v}^n, \mathbf{w}^{n+1}, \mathbf{c}^n) \end{cases} \tag{9}$$

and then $\mathbf{v}^{n+1}, \mathbf{u}_e^{n+1}$ by solving the Bidomain linear system

$$\mathbf{A}_{bid} \begin{pmatrix} \mathbf{v}^{n+1} \\ \mathbf{u}_e^{n+1} \end{pmatrix} = \begin{pmatrix} \mathrm{M}[c_t\mathbf{v}^n - \mathbf{I}^h_{ion}(\mathbf{v}^n, \mathbf{w}^{n+1}, \mathbf{c}^{n+1})] \\ \mathrm{M}\mathbf{I}^{h,e}_{app} \end{pmatrix}, \tag{10}$$

where

$$\mathbf{A}_{bid} = \begin{bmatrix} c_t\mathrm{M} + \mathrm{A}_i & \mathrm{A}_i \\ \mathrm{A}_i & \mathrm{A} \end{bmatrix}. \tag{11}$$

$\mathbf{u}_e^n$, $\mathbf{v}^n$, $\mathbf{w}^n$, $\mathbf{c}^n$, $\mathbf{u}_e^{n+1}$, $\mathbf{v}^{n+1}$, $\mathbf{w}^{n+1}$, $\mathbf{c}^{n+1}$, $\mathbf{I}^h_{ion}$, $\mathbf{I}^{h,e}_{app}$ are the vectors of nodal values of the discrete finite element functions $u_e^{h,n}$, $v^{h,n}$, $w^{h,n}$, $c^{h,n}$, $u_e^{h,n+1}$, $v^{h,n+1}$, $w^{h,n+1}$, $c^{h,n+1}$, i^h_{ion}, $i^{h,e}_{app}$ respectively. As in the continuous model, $\mathbf{v}^{n+1}$ is uniquely determined, while $\mathbf{u}_e^{n+1}$ is determined only up to an additive time-dependent constant chosen by imposing the condition $\mathbf{1}^T\mathrm{M}\mathbf{u}_e^{n+1} = 0$. Hence, at each time step we have to solve the large linear system (10), that is ill-conditioned and increases considerably the computational costs of the simulations.

In order to introduce in the following section the BPX preconditioner for the discrete Bidomain system, we rewrite the discrete formulation of (6) in the compact form:

given $v^{h,n}$, $w^{h,n+1}$, find $u^{h,n+1} \in U^h$ such that

$$a_{bid}(u^{h,n+1}, \hat{u}^h) = (F_i, \hat{v}^h) + (F_e, \hat{u}_e^h) \quad \forall \hat{u}^h = (\hat{v}^h, \hat{u}_e^h) \in V^h \times V^h, \tag{12}$$

with $F_i = c_t\ v^{h,n} - i^h_{ion}(v^{h,n}, w^{h,n+1}, c^{h,n+1})$ and $F_e = i^{h,e}_{app}$.

By defining the linear operator $\mathcal{A}_{bid} : U^h \to U^h$ as

$$((\mathcal{A}_{bid} u^h, \hat{u}^h))_0 = a_{bid}(u^h, \hat{u}^h) \quad \forall \hat{u}^h \in V^h \times V^h,$$

we have that (12) is equivalent to the linear operator equation

$$\mathcal{A}_{bid} u^{h,n+1} = F^h, \tag{13}$$

with right-hand side $F^h \in U^h$ defined as

$$((F^h, \hat{u}^h))_0 = (F_i, \hat{v}^h) + (F_e, \hat{u}_e^h) \quad \forall \hat{u}^h = (\hat{v}^h, \hat{u}_e^h) \in V^h \times V^h.$$

We will construct in the next section the BPX preconditioner for problem (13) and, following the standard abstract BPX theory developed in [35], we will derive optimal convergence rate estimates. We need the following L^2-error estimate for the solutions of (7) and (12), which is obtained by a simple application of the Aubin-Nitsche trick, see [30].

Lemma 3.3. *Let $u = (v, u_e)$ and $u^h = (v^h, u_e^h)$ be the solutions of (7) and (12), respectively. Then the following error estimate holds*

$$||v - v^h||_{L^2(\Omega)} + ||u_e - u_e^h||_{L^2(\Omega)} \leq C\, h\, |||u - u^h|||. \tag{14}$$

4. BPX preconditioner

Preconditioned iterative techniques lead to computationally effective algorithms for the solution of large algebraic systems, which arise in the numerical approximation of PDEs. The Bramble-Pasciak-Xu (BPX) preconditioner is a multilevel preconditioner introduced in [35] for the finite element discretization of scalar elliptic problems. Theoretical results have been obtained initially in the uniform refinement case, but extensions to local refinement in 2D and 3D have also been obtained in [36, 37, 38]. See also [54] for the BPX applied to the discretization of elliptic PDEs on the sphere and the recent paper [55] on BPX preconditioning for isogeometric analysis of elliptic problems.

4.1. Abstract BPX theory

We recall in this section the general abstract construction of the BPX preconditioner, as introduced in [35]. Let

$$\mathcal{M}_1 \subset \mathcal{M}_2 \subset \cdots \subset \mathcal{M}_J \equiv \mathcal{M}, \qquad J \geq 2. \tag{15}$$

be a sequence of nested finite-dimensional spaces. Assume that two inner products, $(\cdot, \cdot)$ and $A(\cdot, \cdot)$, are defined in $\mathcal{M}$ and all its subspaces. For all $k = 1, \ldots, J$ we introduce the following operators:

1. the projection $P_k : \mathcal{M} \longrightarrow \mathcal{M}_k$ defined for $u \in \mathcal{M}$ as

$$A(P_k u, v) = A(u, v) \qquad \forall v \in \mathcal{M}_k;$$

2. the projection $Q_k : \mathcal{M} \longrightarrow \mathcal{M}_k$ defined for $u \in \mathcal{M}$ as

$$(Q_k u, v) = (u, v) \qquad \forall v \in \mathcal{M}_k;$$

3. the operator $A_k : \mathcal{M}_k \longrightarrow \mathcal{M}_k$ defined for $u \in \mathcal{M}_k$ as

$$(A_k u, v) = A(u, v) \qquad \forall v \in \mathcal{M}_k.$$

We indicate $A = A_J$ and define

$$\mathcal{O}_k = \{\phi : \phi = (Q_k - Q_{k-1})\psi,\ \psi \in \mathcal{M}\},$$

with $Q_0 = 0$. With this notation,

$$\mathcal{M}_{j+1} = \mathcal{M}_j \oplus \mathcal{O}_{j+1},$$

so that we can express $\mathcal{M}$ through its multilevel decomposition

$$\mathcal{M} = \bigoplus_{j=1}^{J} \mathcal{O}_j. \tag{16}$$

The BPX preconditioner is defined by

$$B = \sum_{k=1}^{J} \lambda_k^{-1}(Q_k - Q_{k-1}), \tag{17}$$

where λ_k is the spectral radius of A_k.

A more general BPX operator can be obtained by substituting $\lambda_k^{-1} I$ with a symmetric positive definite operator $R_k : \mathcal{M}_k \to \mathcal{M}_k$, i.e.

$$\mathcal{B} = \sum_{k=1}^{J} R_k Q_k. \tag{18}$$

4.2. BPX preconditioner for the Bidomain model

In the Bidomain model notation (see Section 2), the bilinear form $A(\cdot,\cdot)$ and the inner product $(\cdot,\cdot)$ correspond to $a_{bid}(\cdot,\cdot)$ and $((\cdot,\cdot))_0$, respectively. The sequence of nested meshes $\{\mathcal{T}_{h_k}\}$, with $k = 1, ..., J$, is defined using uniform or quasi-uniform meshes with mesh size h_k, where h_1 corresponds to the coarsest mesh and $h_J = h$ to the finest. Since $\{\mathcal{T}_{h_k}\}$ is obtained from a refinement of $\{\mathcal{T}_{h_{k-1}}\}$, it exists a constant $C > 0$ such that

$$h_{k-1} \le C h_k \qquad \forall k = 2, ..., J. \tag{19}$$

On each level $k = 1, \ldots, J$, we define a finite element space V^{h_k}, with $V^{h_J} = V^h$, and the spaces $\tilde{V}^{h_k}$, U^{h_k} as

$$\tilde{V}^{h_k} := \tilde{V}^h \cap V^{h_k},$$
$$U^{h_k} := V^{h_k} \times \tilde{V}^{h_k},$$

so to obtain a sequence of finite element spaces

$$U^{h_1} \subset U^{h_2} \subset \cdots \subset U^{h_J} \equiv U^h.$$

We denote by $\{\phi_i^k\}$ the set of basis functions on the space U^{h_k}.

With the notation of Section 4.1, the operators P_k, Q_k and A_k are

$$P_k : U^h \to U^{h_k} \text{ defined for } u \in U^h \text{ as}$$

$$a_{bid}(P_k u, \tilde{u}) = a_{bid}(u, \tilde{u}) \quad \forall \tilde{u} \in U^{h_k},$$

$$Q_k : U^h \to U^{h_k} \text{ defined for } u \in U^h \text{ as}$$

$$((Q_k u, \tilde{u}))_0 = ((u, \tilde{u}))_0 \quad \forall \tilde{u} \in U^{h_k},$$

$$A_k : U^{h_k} \to U^{h_k} \text{ defined for } u \in U^{h_k} \text{ as}$$

$$((A_k u, \tilde{u}))_0 = a_{bid}(u, \tilde{u}) \quad \forall \tilde{u} \in U^{h_k}.$$

Let us consider the BPX operator $\mathcal{B}$ of the form (18), with $R_k : U^{h_k} \to U^{h_k}$ in the form

$$R_k = h_k^2 I_k, \tag{20}$$

where I_k is the identity on level k. Then the following Theorem holds true.

Theorem 4.1. *The condition number of the Bidomain linear system (13) preconditioned by the BPX preconditioner satisfies*

$$\kappa_2(\mathcal{B}^{1/2} \mathcal{A}_{bid} \mathcal{B}^{1/2}) \leq C,$$

with C independent of the mesh sizes h_k and number of levels J.

Proof. The estimate follows easily from the properties of the Bidomain bilinear form detailed in Section 3 by applying the results obtained in [38].

4.3. Matrix form of the BPX preconditioner

In order to construct the matrix form of the BPX preconditioner, we need to introduce the prolongation and restriction operators among the different grids, see [56]. Since $U^{h_k} \subset U^{h_{k+1}}$, every function ϕ_i^k on the level k can be represented as a linear combination of functions on the level $k+1$. With this refinement relation we can define the prolongation operator $\mathbf{I}_k^{k+1}$ from U^{h_k} to $U^{h_{k+1}}$. The restriction operator $\mathbf{I}_{k+1}^k$ is the inverse of the prolongation one: given a function v^k defined on the fine level $k+1$, the corresponding function on the coarse level k is defined through the transposed operator, i.e. $\mathbf{I}_{k+1}^k = (\mathbf{I}_k^{k+1})^T$. We set also $\mathbf{I}_k^J := \mathbf{I}_{J-1}^J \mathbf{I}_{J-2}^{J-1} \cdots \mathbf{I}_k^{k+1}$ and $\mathbf{I}_J^k := \mathbf{I}_k^{k+1} \mathbf{I}_{k+1}^{k+2} \cdots \mathbf{I}_{J-1}^J$ for the prolongation and restriction operator between arbitrary levels.

The discretized BPX preconditioner has the following matrix form:

$$\mathbf{B} = \sum_{k=1}^{J} h_k^2 \mathbf{I}_k^J \mathbf{I}_J^k.$$

An improvement of this preconditioner is obtained by substituting the scalar factor h_k^2 with $\text{diag}(\mathbf{A}_k)^{-1}$, where $\text{diag}(\mathbf{A}_k)$ indicates the diagonal matrix obtained from the diagonal entries of the stiffness matrix $\mathbf{A}_k$. The diagonal scaling has the same effect of the scaling by levels of h_k^2, but improves the condition number ([55]). Finally, we get the discretized BPX preconditioner

$$\mathbf{B} = \sum_{k=1}^{J} \mathbf{I}_k^J \text{diag}(\mathbf{A}_k)^{-1} \mathbf{I}_J^k.$$

We introduce now a further improvement. Let $\mathbf{A}_1$ be the operator on the coarsest level. If the condition number $\kappa(\mathbf{A}_1)$ is already high on the coarsest level, it can be better to use the exact inverse on the coarsest mesh, i.e. apply

$$\mathbf{B} = \mathbf{I}_1^J \mathbf{A}_1^{-1} \mathbf{I}_J^1 + \sum_{k=2}^{J} \mathbf{I}_k^J \mathrm{diag}(\mathbf{A}_k)^{-1} \mathbf{I}_J^k. \tag{21}$$

Another improvement can be obtained substituting the diagonal scaling on every level with an ILU(0) preconditioning.

5. Numerical results

The numerical results in the two-dimensional case have been obtained using a MATLAB code on a standard desk computer. The 3D simulations have been performed using our FORTRAN code based on the PETSc library of the Argonne National Laboratory [57, 58], run on a single processor of the Nemo Linux cluster at the Department of Mathematics of the University of Milan [59].

The weak formulation of the Bidomain model coupled with the LR1 model is integrated using the semi-implicit finite difference method described in the Section 3. In order to minimize the bandwidth of the stiffness matrix, the unknowns have been reordered writing for each node the $\mathbf{v}_i$ and $\mathbf{u}_e$ components consecutively. The linear system is solved at every step using the preconditioned conjugate method (PCG), using 10^{-6} relative residual reduction as stopping criterion. We use the following preconditioners:

- J level BPX preconditioner, with exact matrix on the coarse level and diagonal matrix on the other levels (in the following BPX(J)-diag), as in (21);
- J level BPX preconditioner, with exact matrix on the coarse level and ILU(0) on the other levels (in the following BPX(J)-ilu).

Domain structure. The domain Ω is a square in 2D and the image of a cartesian slab using ellipsoidal coordinates in 3D, yielding a portion of truncated ellipsoid. The family of truncated ellipsoids is described by the parametric equations

$$\begin{cases} x = a(r)\cos\theta\cos\phi & \phi_{min} \le \phi \le \phi_{max}, \\ y = b(r)\cos\theta\sin\phi & \theta_{min} \le \theta \le \theta_{max}, \\ z = c(r)\sin\theta & 0 \le r \le 1, \end{cases}$$

where $a(r) = a_1 + r(a_2 - a_1)$, $b(r) = b_1 + r(b_2 - b_1)$, $c(r) = c_1 + r(c_2 - c_1)$, and $a_i, b_i, c_i, i = 1, 2$ are given coefficients determining the main axes of the ellipsoid. The fibers rotate intramurally linearly with the depth for a total amount of 90^o proceeding counterclockwise from epicardium to endocardium. More precisely, in a local ellipsoidal reference system $(\mathbf{e}_\phi, \mathbf{e}_\theta, \mathbf{e}_r)$, the fiber direction $\mathbf{a}_l(\mathbf{x})$ at a point $\mathbf{x}$ is given by

$$\mathbf{a}_l(\mathbf{x}) = \mathbf{e}_\phi \cos\alpha(r) + \mathbf{e}_\theta \sin\alpha(r), \quad \text{with} \quad \alpha(r) = \frac{\pi}{2}(1-r) - \frac{\pi}{4}, \qquad 0 \le r \le 1.$$

Mesh hierarchy. In order to build the grids of the BPX(J) preconditioner, in the 2D and 3D structured case of Q_1 finite elements, we start from the coarsest mesh, and then we refine it $J-1$

h	dof	BPX(3)-diag				BPX(3)-ilu			
		κ_2	λ_{max}	λ_{min}	it	κ_2	λ_{max}	λ_{min}	it
0.02	578	9.39	2.92	0.31	19	3.13	3.06	0.98	11
0.01	2178	16.24	3.29	0.20	25	3.20	3.06	0.96	12
0.005	8450	31.21	3.54	0.11	35	3.25	3.15	0.97	12
0.0025	33282	59.72	4.11	0.07	46	3.24	3.18	0.98	12
0.00125	132098	74.66	3.97	0.05	53	3.46	3.43	0.99	13
0.000625	526338	92.20	4.84	0.05	58	3.87	3.72	0.96	14
h	dof	BPX(4)-diag				BPX(4)-ilu			
		κ_2	λ_{max}	λ_{min}	it	κ_2	λ_{max}	λ_{min}	it
0.02	578	12.62	3.87	0.31	21	4.03	4.00	0.99	13
0.01	2178	19.05	4.01	0.21	28	4.13	3.98	0.96	14
0.005	8450	37.28	4.03	0.11	38	3.94	3.87	0.98	14
0.0025	33282	77.39	4.82	0.06	54	3.86	3.90	1.00	13
0.00125	132098	97.83	5.33	0.05	61	4.09	4.10	1.00	14
0.000625	526338	118.70	5.64	0.05	69	4.66	4.60	0.99	16

Table 1: Test 1, optimality with respect to mesh size, 2D structured meshes. 3 and 4 levels BPX-diag and BPX-ilu preconditioners. Mesh size h, degrees of freedom of the Bidomain linear system (dof), average condition number (κ_2), maximal (λ_{max}) and minimal (λ_{min}) eigenvalues of the preconditioned system, and PCG iterations (it) per time step.

times by halving the mesh size in each coordinate direction. In the 2D unstructured case of P_1 finite elements, we start from the coarsest mesh, generated with the PDETool toolbox of MATLAB, and then we refine it $J-1$ times using the routine refinemesh of PDETool.

Conductivity coefficients. The orthotropic conductivity coefficients of the 3D conductivity tensors (1) are

$$\sigma_l^i = 3\cdot 10^{-3}, \quad \sigma_t^i = 3.1525\cdot 10^{-4}, \quad \sigma_n^i = 3.1525\cdot 10^{-5},$$
$$\sigma_l^e = 2\cdot 10^{-3}, \quad \sigma_t^e = 1.3514\cdot 10^{-3}, \quad \sigma_n^e = 6.7570\cdot 10^{-4}.$$

All values are given in $\Omega^{-1}\mathrm{cm}^{-1}$. We recall that in 2D the conductivity tensors (1) become

$$D_{i,e}(\mathbf{x}) = \sigma_l^{i,e}\mathbf{a}_l(\mathbf{x})\mathbf{a}_l^T(\mathbf{x}) + \sigma_t^{i,e}\mathbf{a}_t(\mathbf{x})\mathbf{a}_t^T(\mathbf{x}).$$

Stimulation site, initial conditions and boundary conditions. The depolarization process starts by applying a stimulus of $I_{app}^e = -200$ mA/cm^3, lasting 1 ms, to an area of about 0.02×0.02 cm^2 in 2D ($0.02\times 0.02\times 0.02$ cm^3 in 3D) at the center of the square domain in 2D or at the center of the endocardial surface (the interior surface of the truncated ellipsoid) in 3D. Initial conditions are the resting values for all potentials and gating variables in the LR1 model, with boundary conditions for insulated tissues. Except the last test on the whole cardiac beat, in all the other tests the model is run for 40 time steps of 0.05 ms after the stimulation, i.e. for a total time interval of 2 ms during the excitation phase.

5.1. Test 1: optimality with respect to the mesh size, 2D structured meshes

The aim of this test is to study the performance of the BPX preconditioner when decreasing the mesh size h. The number of levels J considered is 3 and 4. The 2D domain is a square of

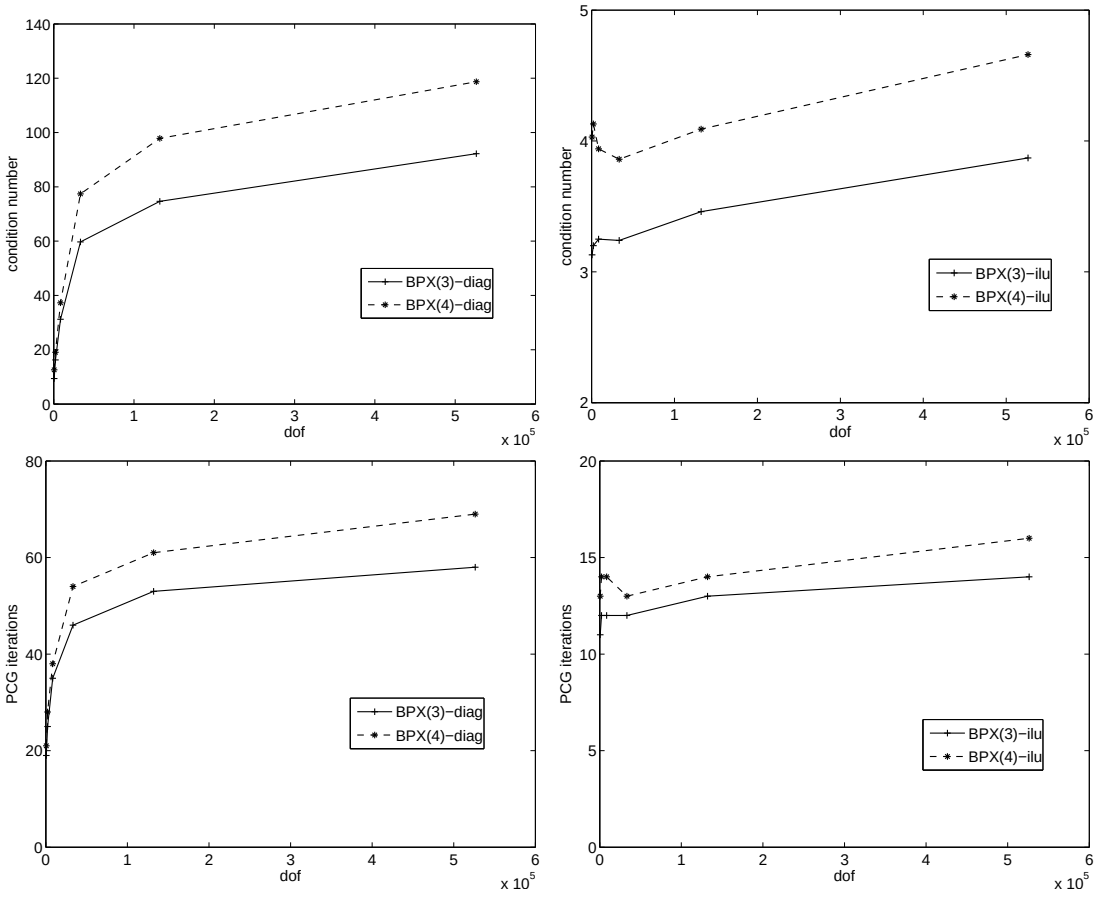

Figure 1: Test 1, optimality with respect to mesh size, 2D structured meshes. Plots of condition numbers and iteration counts from the data reported in Table 1.

dimension $0.32 \times 0.32\ cm^2$, discretized by six different grids of Q_1 finite elements. The mesh size of the coarsest grid is $0.02\ cm$, while that of the finest one is $0.000625\ cm$. As a result, the degrees of freedom (dof) of the Bidomain linear system vary from 578 in the coarsest case to 526338 in the finest one.

Table 1 reports the average condition number, maximal and minimal eigenvalues of the preconditioned system, and PCG iteration counts per time step. The condition number and PCG iteration counts are also plotted in Fig. 1 for better clarity.

The results show that, in the BPX-diag case, both condition numbers and iteration counts increase when refining h, but, asymptotically, as also confirmed by the plots in Fig. 1, they seem to be bounded from above, according to the estimate in Theorem 4.1. The independence of the condition number with respect to the mesh size, thus the optimality of the preconditioner, is instead clear in the BPX-ilu case. The significant improvement of the BPX-ilu preconditioner with respect to the BPX-diag is mainly due to the increase of the minimal eigenvalue, which is close to 1.

J	BPX(J)-diag				BPX(J)-ilu			
	κ_2	λ_{max}	λ_{min}	it	κ_2	λ_{max}	λ_{min}	it
2	11.75	3.89	0.33	21	2.34	2.17	0.93	9
3	14.91	4.94	0.33	25	3.59	3.39	0.94	11
4	15.70	5.26	0.33	26	4.82	4.56	0.95	13
5	17.06	5.72	0.33	27	5.93	5.61	0.95	15
6	18.23	6.12	0.34	28	7.01	6.64	0.95	16
7	19.67	6.61	0.34	29	7.99	7.59	0.95	18
8	22.19	7.47	0.34	30	8.80	8.42	0.96	19
9	25.35	8.49	0.33	31	9.97	9.40	0.94	19
10	27.93	9.38	0.34	32	10.85	10.30	0.95	20

Table 2: Test 2, increasing the number of levels, 2D structured meshes. J-level BPX-diag and BPX-ilu preconditioners. Number of levels J, average condition number (κ_2), maximal (λ_{max}) and minimal (λ_{min}) eigenvalues of the preconditioned system, and PCG iterations (it) per time step.

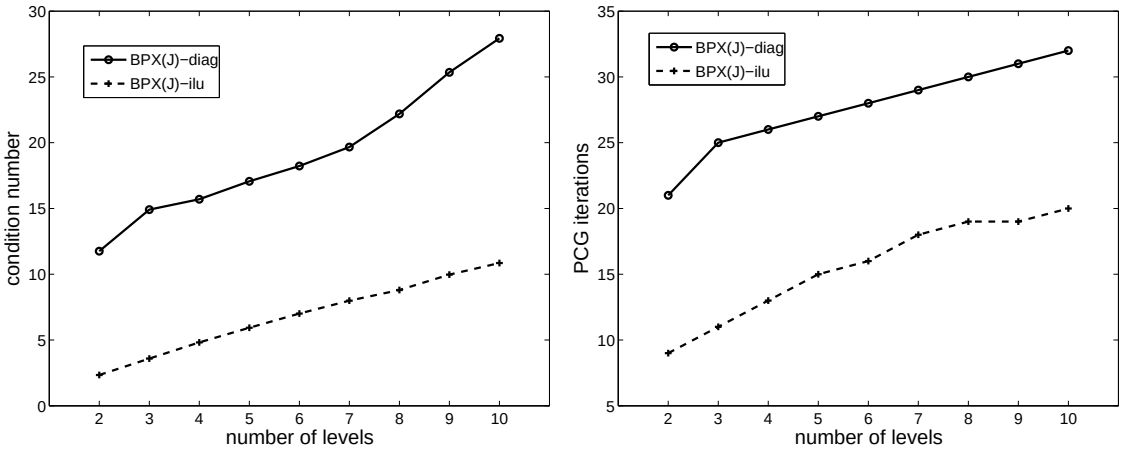

Figure 2: Test 2, increasing the number of levels, 2D structured meshes. Plots of condition numbers and iteration counts from the data reported in Table 2.

h	dof	BPX(2)-diag				BPX(2)-ilu			
		κ_2	λ_{max}	λ_{min}	it	κ_2	λ_{max}	λ_{min}	it
0.0285	2709	12.27	3.72	0.30	16	2.37	1.96	0.81	7
0.0142	10665	21.56	4.11	0.19	21	2.67	2.04	0.75	8
0.0071	42321	33.17	4.22	0.12	26	3.11	2.14	0.67	9
0.0035	168609	35.00	4.25	0.12	27	3.41	2.19	0.63	10
h	dof	BPX(3)-diag				BPX(3)-ilu			
		κ_2	λ_{max}	λ_{min}	it	κ_2	λ_{max}	λ_{min}	it
0.0285	2709	17.42	5.16	0.29	19	3.38	2.85	0.82	8
0.0142	10665	30.85	5.93	0.19	26	3.74	2.85	0.74	9
0.0071	42321	51.10	6.26	0.12	32	4.31	2.91	0.66	11
0.0035	168609	67.24	6.38	0.09	37	4.76	2.96	0.61	12

Table 3: Test 3, optimality with respect to mesh size, 2D unstructured meshes. 2 and 3 levels BPX-diag and BPX-ilu preconditioners. Mesh size h, degrees of freedom of the Bidomain linear system (dof), average condition number (κ_2), maximal (λ_{max}) and minimal (λ_{min}) eigenvalues of the preconditioned system, and PCG iterations (it) per time step.

5.2. Test 2: increasing the number of levels, 2D structured mesh

In this second test, we study the behavior of the BPX preconditioner with respect to the number of levels J. The domain is a square of dimension 5.12×5.12 cm^2, discretized by a Q_1 structured grid of 512×512 finite elements, thus the mesh size is $h = 0.01$ cm. The total dof of the Bidomain linear system are 526338. The number of levels varies from 2 to 10.

The results in Table 2, also confirmed by the plots in Fig. 2, show that, even though the minimal eigenvalue of the preconditioned operator is bounded from below away from zero irrespective of the number of levels J, the maximal eigenvalue grows weakly with J. As a result, the condition number κ_2 increases, but, since the growth rate reduces when J increases, κ_2 seems to be aymptotically bounded, as predicted by Theorem 4.1.

5.3. Test 3: optimality with respect to mesh size, 2D unstructured meshes

We study here the performance of the BPX preconditioner when decreasing the mesh size h, on 2D unstructured meshes. The number of levels J considered is 2 and 3. The 2D domain is a square, discretized by four different grids of P_1 finite elements. The mesh size of the coarsest grid is 0.0285 cm, while that of the finest one is 0.0035 cm. As a result, the number of dof of the Bidomain linear system varies from 2709 in the coarsest case to 168609 in the finest one.

Table 3 reports the average condition number, maximal and minimal eigenvalues of the preconditioned system, and PCG iteration counts per time step.

As in Test 1, the independence of the BPX preconditioner on the mesh size is much more clear in the BPX-ilu case than in the BPX-diag case, which does not seem to be in the asymptotic behavior, yet.

5.4. Test 4: increasing number of levels, 2D unstructured mesh

This test is devoted to the study of the behavior of the BPX preconditioner with respect to the number of levels J in the case of 2D unstructured meshes. The domain is a square discretized by

J	BPX(J)-diag				BPX(J)-ilu			
	κ_2	λ_{max}	λ_{min}	it	κ_2	λ_{max}	λ_{min}	it
2	33.17	4.22	0.12	26	3.11	2.14	0.67	9
3	51.10	6.26	0.12	32	4.31	2.91	0.66	11
4	59.86	7.36	0.12	36	5.31	3.58	0.66	12
5	65.07	8.00	0.12	37	6.34	4.27	0.66	13

Table 4: Test 4, increasing the number of levels, 2D unstructured meshes. J-level BPX-diag and BPX-ilu preconditioners. Number of levels J, average condition number (κ_2), maximal (λ_{max}) and minimal (λ_{min}) eigenvalues of the preconditioned system, and PCG iterations (it) per time step.

h	dof	BPX(3)-diag				BPX(3)-ilu			
		κ_2	λ_{max}	λ_{min}	it	κ_2	λ_{max}	λ_{min}	it
0.02	1458	15.71	2.76	0.18	23	3.13	3.11	0.99	11
0.01	9826	21.68	3.16	0.15	27	3.20	3.14	0.98	11
0.005	71874	35.27	3.30	0.09	35	3.46	3.32	0.96	11
0.0025	549250	46.30	3.51	0.08	39	3.59	3.49	0.97	11
h	dof	BPX(4)-diag				BPX(4)-ilu			
		κ_2	λ_{max}	λ_{min}	it	κ_2	λ_{max}	λ_{min}	it
0.02	1458	16.35	3.72	0.23	23	3.87	3.85	1.00	13
0.01	9826	22.99	3.73	0.16	28	4.26	4.12	0.97	13
0.005	71874	38.94	4.11	0.11	36	4.44	4.32	0.97	13
0.0025	549250	55.94	4.36	0.08	41	4.35	4.29	0.98	12

Table 5: Test 5, optimality with respect to mesh size, 3D structured meshes. 3 and 4 levels BPX-diag and BPX-ilu preconditioners. Mesh size h, degrees of freedom of the Bidomain linear system (dof), average condition number (κ_2), maximal (λ_{max}) and minimal (λ_{min}) eigenvalues of the preconditioned system, and PCG iterations (it) per time step.

P_1 finite elements, with mesh size $h = 0.0035$ cm. The total number of unknowns of the Bidomain linear system is 168609. The number of levels varies from 2 to 5.

The results in Table 4 still show, as in Test 2, a weak growth of the condition number κ_2 with the number of levels J, but, since the growth rate reduces when J increases, especially for the BPX-diag preconditioner, κ_2 should be asymptotically bounded.

5.5. Test 5: optimality with respect to mesh size, 3D structured meshes

We study the behavior of the BPX preconditioner when decreasing the mesh size h in a three-dimensional slab domain, modeling a small portion of ventricular tissue of dimension $0.16 \times 0.16 \times 0.16$ cm^3. The number of levels J considered is 3 and 4. The domain is discretized by four different grids of Q_1 finite elements. The mesh size of the coarsest grid is 0.02 cm, while that of the finest one is 0.0025 cm. As a result, the degrees of freedom (dof) of the Bidomain linear system vary from 1458 in the coarsest case to 549250 in the finest one.

J	BPX(J)-diag				BPX(J)-ilu			
	κ_2	λ_{max}	λ_{min}	it	κ_2	λ_{max}	λ_{min}	it
2	13.93	2.24	0.16	23	2.20	2.06	0.94	9
3	13.78	2.89	0.21	23	3.14	3.06	0.97	11
4	15.32	4.15	0.27	25	4.17	4.08	0.98	13
5	20.43	5.28	0.26	28	5.16	5.10	0.99	15
6	24.61	6.31	0.26	30	6.16	5.98	0.97	16

Table 6: Test 6, increasing the number of levels, 3D structured meshes. J-level BPX-diag and BPX-ilu preconditioners. Number of levels J, average condition number (κ_2), maximal (λ_{max}) and minimal (λ_{min}) eigenvalues of the preconditioned system, and PCG iterations (it) per time step.

Table 5 reports the average condition number, maximal and minimal eigenvalues of the preconditioned system, and PCG iteration counts per time step.

The results show that, in the BPX-diag case, both condition numbers and iteration counts increase when refining h, but asymptotically they seem to be bounded from above, according to the estimate in Theorem 4.1. The independence of the condition number with respect to the mesh size, thus the optimality of the preconditioner, is instead clear in the BPX-ilu case. The significant improvement of the BPX-ilu preconditioner with respect to the BPX-diag is mainly due to the increase of the minimal eigenvalue, which is close to 1.

5.6. Test 6: increasing the number of levels, 3D structured meshes

We test here the BPX preconditioner on a 3D truncated ellipsoidal domain when the number of levels J increases. The parameters of the ellipsoidal domain are $\phi_{min} = -\frac{\pi}{8},\ \phi_{max} = \frac{\pi}{8}, \theta_{min} = -\frac{\pi}{8},\ \theta_{max} = 0, a_1 = b_1 = 1.5, a_2 = b_2 = 2.7, c_1 = 4.4, c_2 = 5.\ a_i, b_i, c_i,\ i = 1, 2$ are expressed in cm. The fine mesh is fixed and consists of $96 \times 96 \times 48$ Q_1 finite elements, yielding a mesh size of about 0.01 cm. The total dof of the Bidomain linear system are 922082. The number of levels varies from 2 to 6.

The results in Table 6 show that, as in the previous Tests 2 and 4, the condition numbers of both the BPX-diag and BPX-ilu preconditioned systems grow weakly with J, but the behavior seems to be asymptotically bounded.

5.7. Test 7: robustness with respect to jumps in the conductivity coefficients, 3D structured meshes

An important pathological situation that can be studied by numerical simulation based on the Bidomain model is the presence of myocardial ischemia, which is the most common cause of ventricular fibrillation and consequent heart failure. In the ischemic regions, it is experimentally observed a strong reduction of the conduction velocity of the electric signal, due to a decrease of *gap junction* coupling across myocytes. This phenomenon is modeled at macroscopic level by a reduction of the intracellular conductivity values $\sigma^i_{l,t,n}$ inside the ischemic region, leading to a jump of these parameters across the ischemic boundary. Thus, an effective preconditioner for the Bidomain system should be robust with respect to such jumps.

The domain considered in this case is a slab of dimensions $0.96 \times 0.96 \times 0.48$ cm^3, with a transmural ischemic region of dimensions $0.32 \times 0.32 \times 0.16$ cm^3 located at the center of the slab. The portion of tissue is discretized by a cartesian grid of $96 \times 96 \times 48$ Q_1 finite elements (922082

ρ	BPX(3)-diag				BPX(3)-ilu			
	κ_2	λ_{max}	λ_{min}	it	κ_2	λ_{max}	λ_{min}	it
1	40.83	3.04	7.46e-2	37	3.27	3.07	9.38e-1	12
10	39.60	3.05	7.72e-2	37	3.80	3.51	9.23e-1	12
100	39.65	3.13	7.90e-2	38	3.90	3.60	9.23e-1	12
1000	39.68	3.14	7.93e-2	38	3.91	3.61	9.23e-1	12

Table 7: Test 7, robustness with respect to jumps in the conductivity coefficients, 3D structured meshes. 3-level BPX-diag and BPX-ilu preconditioners. Jump parameter ρ, average condition number (κ_2), maximal (λ_{max}) and minimal (λ_{min}) eigenvalues of the preconditioned system, and PCG iterations (it) per time step.

proc	BPX(4)-diag				BPX(4)-ilu			
	κ_2	it	time (s)	speedup	κ_2	it	time (s)	speedup
64	20.71	29	30.28	-	8.31	19	29.47	-
128	20.71	29	15.41	1.96 (2)	8.25	19	15.17	1.94 (2)
256	20.71	29	8.38	3.61 (4)	8.29	19	8.00	3.68 (4)
512	20.71	29	4.74	6.39 (8)	8.28	19	4.34	6.79 (8)
1024	20.71	29	3.24	9.35 (16)	8.20	19	2.69	10.95 (16)

Table 8: Test 8, parallel performance, 3D structured meshes. 4-level BPX-diag and BPX-ilu preconditioners. Number of processors (proc), average condition number (κ_2), PCG iterations (it), CPU time in seconds per time step, and parallel speedup. In brackets is reported the ideal speedup.

dof). The ischemic condition is modeled by increasing the extracellular concentration of potassium in the LR1 model from 5.4 mM (control) to 20 mM (ischemia) (see [60]) and scaling the conductivity coefficients $\sigma^i_{l,t,n}$ in the ischemic region as follows:

$$\sigma^{i,isch}_{l,t,n} = \sigma^i_{l,t,n}/\rho,$$

where ρ is a jump parameter.

The results in Table 7 show that both the 3-level BPX-diag and BPX-ilu preconditioners are robust with respect to the jump considered, since the condition number of the preconditioned system and the PCG iteration counts remain bounded increasing the jump value.

5.8. Test 8: parallel performance, 3D structured meshes

We perform a strong scaling test to study the parallel performance of the BPX-diag and BPX-ilu preconditioners. A truncated ellipsoidal domain is considered, discretized by a Q_1 finite element grid of $512 \times 512 \times 96$ elements, yielding a Bidomain linear system of 51 054 786 dof. The parameters of the ellipsoidal domain are $\phi_{min} = -\frac{\pi}{2},\ \phi_{max} = \frac{\pi}{2}, \theta_{min} = -\frac{3}{8}\pi,\ \theta_{max} = \frac{\pi}{8}, a_1 = b_1 = 1.5, a_2 = b_2 = 2.7, c_1 = 4.4, c_2 = 5.$ $a_i, b_i, c_i,\ i = 1, 2$ are expressed in cm. The number of processors varies from 64 to 1024 and the number of levels J of the BPX preconditioners is set to 4. The parallel speedup is computed with respect to the 64 processor run, thus the ideal speedup ranges from 1 to 16. The code was run on the IBM-BlueGene Q cluster *Fermi* of the CINECA laboratory (www.cineca.it).

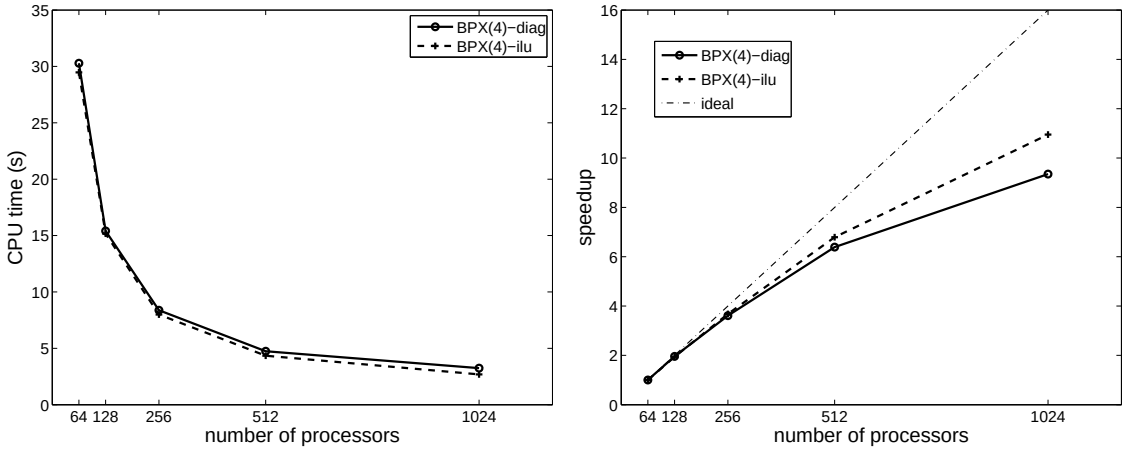

Figure 3: Test 8, parallel performance, 3D structured meshes. 4-level BPX-diag and BPX-ilu preconditioners. Plot of average CPU time in seconds per time step (left) and parallel speedup (right) with respect to the number of processors.

The results reported in Table 8 and Fig. 3 show that both the BPX(4)-diag and BPX(4)-ilu preconditioners are scalable, with a good speedup up to 512 processors, slightly deteriorating in the 1024 processors run, because at this point the local problems are too small and the communication costs prevail.

5.9. Test 9: influence of the membrane model, 3D structured meshes

We study here the influence of membrane models on the performance of the BPX preconditioner. A strong scaling test is run on the same truncated ellipsoidal domain of Test 6, discretized by a Q_1 finite element grid of $96 \times 96 \times 48$ elements (922082 dof). The number of processors varies from 1 to 24 and the number of levels J of the BPX preconditioners is set to 4. The membrane models considered are the LR1 model (7 ODEs) as in the other tests, the ten Tusscher model ([61], 18 ODEs), for human ventricular myocytes, and the Shannon model ([62], 38 ODEs), for rabbit ventricular myocytes. This test is run on the Nemo Linux cluster at the Department of Mathematics of the University of Milan [59].

The results reported in Table 9 show that the behavior of the BPX preconditioners, both in terms of PCG iterations and CPU times (time_{ls}), is independent of the choice of the membrane model. Moreover, the solution of the membrane models is completely scalable and the CPU times (time_m) clearly increase with the complexity of the membrane model.

5.10. Test 10: complete cardiac cycle simulation, 3D structured meshes

In this last test, a complete heartbeat (400 ms) is simulated in the truncated ellipsoidal domain of Test 6, discretized by a Q_1 finite element grid of $96 \times 96 \times 48$ elements (922082 dof). The time step size is changed according to the adaptive strategy described in [20], yielding a total amount of 2200 time steps. Fig. 4 reports the contour plots of the transmembrane (v) and extracellular (u_e) potential distributions on the endocardial and mid-myocardial surfaces, at 10, 20 and 30 ms after the onset of stimulation.

BPX(4)-diag									
proc	LR1			ten Tusscher			Shannon		
	it	$time_{ls}$	$time_m$	it	$time_{ls}$	$time_m$	it	$time_{ls}$	$time_m$
1	41	47.71	4.05e-1	41	46.87	9.68e-1	41	47.57	1.35
2	41	24.10	2.04e-1	41	23.55	4.93e-1	41	23.30	6.90e-1
4	41	12.35	1.03e-1	41	12.14	2.49e-1	41	12.33	3.56e-1
8	41	6.47	5.43e-2	41	6.39	1.27e-1	41	6.42	1.88e-1
16	41	3.09	2.80e-2	41	3.08	6.99e-2	41	3.08	9.77e-2
24	41	2.13	1.85e-2	41	2.11	4.36e-2	41	2.11	6.30e-2
BPX(4)-ilu									
proc	LR1			ten Tusscher			Shannon		
	it	$time_{ls}$	$time_m$	it	$time_{ls}$	$time_m$	it	$time_{ls}$	$time_m$
1	14	38.79	4.05e-1	14	38.29	9.68e-1	14	38.64	1.35
2	17	19.59	2.04e-1	17	19.24	4.93e-1	17	19.42	6.90e-1
4	17	10.05	1.03e-1	17	9.97	2.49e-1	17	10.06	3.56e-1
8	19	5.26	5.41e-2	18	5.22	1.27e-1	18	5.24	1.88e-1
16	19	2.61	2.80e-2	18	2.60	6.98e-2	18	2.60	9.74e-2
24	19	1.76	1.86e-2	18	1.74	4.36e-2	18	1.76	6.29e-2

Table 9: Test 9, influence of the membrane model on the linear solver, 3D structured meshes. 4-level BPX-diag and BPX-ilu preconditioners. Luo-Rudy I (LR1), ten Tusscher and Shannon membrane models. Number of processors (proc), average PCG iterations (it) per time step, average CPU time in seconds for solving the Bidomain linear system ($time_{ls}$) and the membrane model ($time_m$) per time step.

prec.	κ_2	λ_{max}	λ_{min}	it	Tit	time (s)	Ttime (s)		
ILU	636.76	1.57	2.77e-3	64	142757	35.89	22 h	6 m	5 s
AMG	1.22	1.01	8.25e-1	5	11085	36.33	22 h	22 m	35 s
BPX(3)-diag	37.64	3.17	9.54e-2	30	66547	37.71	23 h	13 m	16 s
BPX(3)-ilu	7.32	3.64	6.67e-1	13	28965	28.71	17 h	41 m	1 s
BPX(4)-diag	43.03	4.25	1.16e-1	31	68831	23.37	14 h	23 m	22 s
BPX(4)-ilu	9.51	4.80	6.74e-1	15	33493	39.11	24 h	5 m	3 s

Table 10: Test 10, complete cardiac cycle simulation, 3D structured meshes. Performance comparison of ILU, AMG, BPX(3)-diag, BPX(3)-ilu, BPX(4)-diag and BPX(4)-ilu preconditioners. Average (per time step) condition number (κ_2), maximal (λ_{max}) and minimal (λ_{min}) eigenvalues of the preconditioned system, average (per time step) and total PCG iterations (it and Tit, respectively), average (per time step) CPU time (time) in seconds and total CPU time (Ttime) in hours (h), minutes (m) and seconds (s) for solving the Bidomain linear systems.

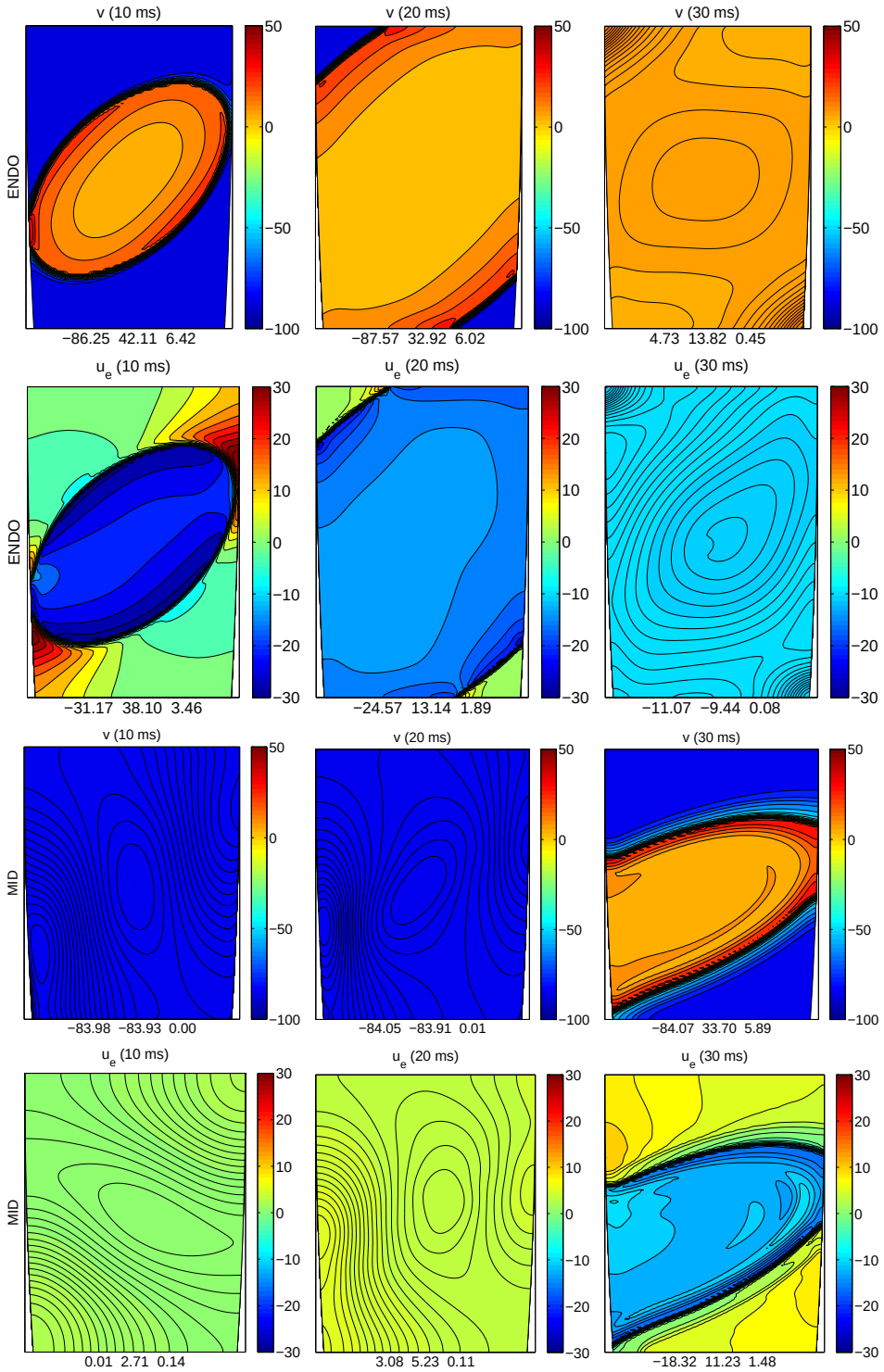

Figure 4: Test 10, complete cardiac cycle simulation, 3D structured meshes. Contour plots of the transmembrane (v) and extracellular (u_e) potential distributions on the endocardial (ENDO) and mid-myocardial (MID) surfaces of the truncated ellipsoidal domain modeling a portion of ventricle, at 10, 20 and 30 ms after the onset of stimulation. Below each plot are reported the minimum, maximum and contour step in mV of the displayed map.

We compare the BPX-diag and BPX-ilu preconditioners with the ILU(0) preconditioner and the default setting of the Algebraic Multigrid (AMG) BoomerAMG [63] preconditioner, provided within the HYPRE library [64] of the Lawrence Livermore National Laboratory. The number of levels considered for the BPX preconditioners is 3 and 4.

The results in Table 10 show that the best performance in terms of condition numbers and PCG iterations counts is achieved by the AMG preconditioner, but in terms of CPU times the BPX(3)-ilu and BPX(4)-diag preconditioners are the most effective. In particular, in terms of CPU times, the BPX(4)-diag preconditioner attains the overall best performance, being about 35% faster than the ILU(0) and AMG preconditioners.

6. Conclusions

We have constructed, analyzed and numerically tested a BPX preconditioner for the Bidomain system of electrocardiology. By applying the abstract BPX theory, we have proved that the condition number of the BPX-preconditioned Bidomain system does not depend on the mesh size h and on the number of levels J (optimality). These theoretical results have been validated by two- and three-dimensional numerical tests on both structured and unstructured grids. Moreover, we have shown that, in a full heartbeat simulation on a three-dimensional wedge of ventricular tissue, the BPX preconditioner is about 35% faster in terms of CPU times than ILU(0) and the default setting of the BoomerAMG preconditioner. We remark that better results in terms of CPU times with AMG could be obtained with other choices of the parameters and on different computing platforms.

Limitations of this work include the use of idealized ventricular geometries instead of anatomically more accurate domains and the use of the LR1 ionic model instead of physiologically more accurate membrane models. Moreover, to further validate the performance of the BPX preconditioner, a more extensive comparison with other methods should be planned in future works.

Appendix: general structure of membrane models

The first membrane model was developed by Hodgkin and Huxley in the celebrated paper [65] for the nerve action potential. Based on their pioneering work, several membrane models for cardiac cells have been developed, see e.g. [47, 66, 67]. According to the formalism of the Hodgkin-Huxley (HH) model, the ionic current through channels of the membrane is modulated by the transmembrane potential $v = u_i - u_e$, by gating variables $w := (w_1, \ldots, w_{N_w})$ and by ionic intracellular concentration variables $c := (c_1, \ldots, c_{N_c})$. In the membrane models of HH type, the ionic current has the following general structure

$$I_{ion}(v, w, c) = \sum_{k=1}^{N} G_k(v, c) \prod_{j=1}^{N_w} w_j^{p_{j_k}} (v - v_k(c)) + I_n(v, w, c),$$

where N is the number of ionic currents, G_k is the membrane conductance and v_k is the reversal potential for the k-th current, p_{j_k} are integers and I_n accounts for time independent ionic fluxes.

The dynamics of the gating variables w is described in the HH formalism by a system of ODEs having the following structure

$$\begin{cases} \dfrac{dw_j}{dt} = R_j(v, w) = \alpha_j(v)(1 - w_j) - \beta_j(v) w_j \\ w_j(0) = w_{j,0} \\ \alpha_j, \quad \beta_j > 0, \quad 0 \le w_j \le 1, \quad j = 1, ..., N_w. \end{cases} \tag{22}$$

The dynamics of the ionic concentration variables c is described by the additional system of ODEs

$$\begin{cases} \dfrac{dc_j}{dt} = S_j(v,w,c) = -\dfrac{I_{c_j}(v,w)\cdot A_{cap}}{V_{c_j}\cdot z_{c_j}\cdot F} \\ c_j(0) = c_{j,0} \\ j = 1,...,N_c, \end{cases} \tag{23}$$

where I_{c_j} is the sum of ionic currents carrying ion c_j, A_{cap} is the capacitive membrane area, V_{c_j} is the volume of the compartment where c_j is updated, z_{c_j} is the valence of ion c_j and F is the Faraday constant.

The transmembrane current

$$I_m = C_m\frac{dv}{dt} + I_{ion}(v,w,c)$$

is the sum of the capacitive current, associated with the membrane lipidic bilayer and of the ionic current I_{ion}. Since I_m must balance the applied current I_{app}, then the evolution of the transmembrane potential of a single myocyte is given by the following system of ODEs

$$\begin{cases} C_m\dfrac{dv}{dt} + I_{ion}(v,w,c) = I_{app} \\ \dfrac{dw}{dt} - R(v,w) = 0, \\ \dfrac{dc}{dt} - S(v,w,c) = 0 \\ v(0) = v_0, \quad w(0) = w_0, \quad c(0) = c_0, \end{cases} \tag{24}$$

where C_m, I_{ion}, and I_{app} are the surface capacitance, the ionic current of the membrane and the applied current per unit area of the membrane surface, respectively.

Acknowledgements

The authors were partially supported by grants of MIUR (PRIN 201289A4LX_002) and of INdAM (INdAM-GNCS_2014). We also thank Piero Colli Franzone and Luca F. Pavarino for many helpful discussions and suggestions.

References

[1] M. Murillo, X.-C. Cai, A fully implicit parallel algorithm for simulating the non-linear electrical activity of the heart, Numer. Linear Algebra Appl. 11 (2-3) (2004) 261–277.

[2] M. Munteanu, L. F. Pavarino, Decoupled schwarz algorithms for implicit discretization of nonlinear monodomain and bidomain systems, Math. Mod. Meth. Appl. Sci. 19 (7) (2009) 1065–1097.

[3] M. Munteanu, L. F. Pavarino, S. Scacchi, A scalable Newton-Krylov-Schwarz method for the Bidomain reaction-diffusion system, SIAM J. Sci. Comput. 31 (5) (2009) 3861–3883.

[4] S. Scacchi, A multilevel hybrid newton-krylov-schwarz method for the bidomain model of electrocardiology, Comput. Meth. Appl. Mech. Engrg. 200 (5-8) (2011) 717–725.

[5] M. Boulakia, S. Cazeau, M. A. Fernandez, J.-F. Gerbeau, N. Zemzemi, Mathematical modeling of electrocardiograms: a numerical study, Ann. Biomed. Engrg. 38 (3) (2010) 1071–1097.

[6] P. Colli Franzone, L. F. Pavarino, B. Taccardi, Simulating patterns of excitation, repolarization and action potential duration with cardiac bidomain and monodomain models, Math. Biosci. 197 (1) (2005) 35–66.

[7] P. Colli Franzone, L. F. Pavarino, S. Scacchi, A comparison of coupled and uncoupled solvers for the cardiac bidomain model, ESAIM-Math. Mod. Numer. Anal. 47 (4) (2013) 1017–1035.

[8] M. Ethier, Y. Bourgault, Semi-implicit time-discretization schemes for the bidomain model, SIAM J. Numer. Anal. 46 (5) (2008) 2443–2468.

[9] S. Linge, J. Sundnes, M. Hanslien, G. T. Lines, A. Tveito, Numerical solution of the bidomain equations, Phil. Trans. R. Soc. A 367 (1895) (2009) 1931–1950.

[10] J. Southern, G. Plank, E. J. Vigmond, J. P. Whiteley, Solving the coupled system improves computational efficiency of the bidomain equations, IEEE Trans. Biomed. Engrg. 56 (10) (2009) 2404–2412.

[11] J. Sundnes, G. T. Lines, A. Tveito, An operator splitting method for solving the bidomain equations coupled to a volume conductor model for the torso, Math. Biosci. 194 (2) (2005) 233–248.

[12] E. J. Vigmond, R. Weber dos Santos, A. J. Prassl, M. Deo, G. Plank, Solvers for the cardiac bidomain equations, Progr. Biophys. Molec. Biol. 96 (2008) 3–18.

[13] J. P. Whiteley, An efficient numerical technique for the solution of the monodomain and bidomain equations, IEEE Trans. Biomed. Engrg. 53 (2006) 2139–2147.

[14] P. Pathmanathan, M. O. Bernabeu, R. Bordas, J. Cooper, A. Garny, J. M. Pitt-Francis, J. P. Whiteley, D. J. Gavaghan, A numerical guide to the solution of the bidomain equations of cardiac electrophysiology, Progr. Biophys. Molec. Biol. 102 (2010) 136–155.

[15] M. Potse, B. Dubé, J. Richer, A. Vinet, R. M. Gulrajani, A comparison of monodomain and bidomain reaction-diffusion models for action potential propagation in the human heart, IEEE Trans. Biomed. Engrg. 53 (12) (2006) 2425–2435.

[16] M. Pennacchio, V. Simoncini, Efficient algebraic solution of reaction-diffusion systems for the cardiac excitation process, J. Comput. Appl. Math. 145 (1) (2002) 49–70.

[17] M. O. Bernabeu, P. Pathmanathan, J. Pitt-Francis, D. Kay, Stimulus protocol determines the most computationally efficient preconditioner for the bidomain equations, IEEE Trans. Biomed. Engrg. 57 (12) (2010) 2806–2815.

[18] M. Pennacchio, V. Simoncini, Algebraic multigrid preconditioners for the bidomain reaction-diffusion system, Appl. Numer. Math. 59 (2009) 3033–3050.

[19] M. Pennacchio, V. Simoncini, Fast structured amg preconditioning for the bidomain model in electrocardiology, SIAM J. Sci. Comput. 33 (2) (2011) 721–745.

[20] P. Colli Franzone, L. F. Pavarino, A parallel solver for reaction-diffusion systems in computational electrocardiology, Math. Mod. Meth. Appl. Sci. 14 (6) (2004) 883–911.

[21] E. J. Vigmond, F. Aguel, N. A. Trayanova, Computational techniques for solving the bidomain equations in three dimensions, IEEE Trans. Biomed. Engrg. 49 (11) (2002) 1260–1269.

[22] L. Gerardo-Giorda, L. Mirabella, F. Nobile, M. Perego, A. Veneziani, A model-based block-triangular preconditioner for the bidomain system in electrocardiology, J. Comp. Phys. 228 (10) (2009) 3625–3639.

[23] L. Gerardo-Giorda, L. Mirabella, Spectral analysis of a block-triangular preconditioner for the bidomain system in electrocardiology, Elec. Trans. Numer. Anal. 39 (2012) 186–201.

[24] L. Gerardo-Giorda, M. Perego, A. Veneziani, Optimized schwarz coupling of bidomain and monodomain models in electrocardiology, ESAIM-Math. Mod. Numer. Anal. 45 (2011) 309–334.

[25] L. Gerardo-Giorda, M. Perego, Optimized schwarz methods for the bidomain system in electrocardiology, ESAIM-Math. Mod. Numer. Anal. 47 (2) (2013) 583–608.

[26] J. Sundnes, G. T. Lines, K. A. Mardal, A. Tveito, Multigrid block preconditioning for a coupled system of partial differential equations modeling the electrical activity in the heart, Comput. Meth. Biomech. Biomed. Engrg. 5 (6) (2002) 397–409.

[27] R. Weber dos Santos, G. Plank, S. Bauer, E. J. Vigmond, Parallel multigrid preconditioner for the cardiac bidomain model, IEEE Trans. Biomed. Engrg. 51 (11) (2004) 1960–1968.

[28] T. M. Austin, M. L. Trew, A. J. Pullan, Solving the cardiac bidomain equations for discontinuous conductivities, IEEE Trans. Biomed. Engrg. 53 (7) (2006) 1265–1272.

[29] G. Plank, M. Liebmann, R. Weber dos Santos, E. J. Vigmond, G. Haase, Algebraic multigrid preconditioner for the cardiac bidomain model, IEEE Trans. Biomed. Engrg. 54 (4) (2007) 585–596.

[30] L. F. Pavarino, S. Scacchi, Multilevel additive schwarz preconditioners for the bidomain reaction-diffusion system, SIAM J. Sci. Comput. 31 (1) (2008) 420–443.

[31] L. F. Pavarino, S. Scacchi, Parallel multilevel schwarz and block preconditioners for the bidomain parabolic-parabolic and parabolic-elliptic formulations, SIAM J. Sci. Comput. 33 (4) (2011) 1897–1919.

[32] S. Scacchi, A hybrid multilevel schwarz method for the bidomain model, Comput. Meth. Appl. Mech. Engrg. 197 (2008) 4051–4061.

[33] S. Zampini, Balancing Neumann-Neumann methods for the cardiac Bidomain model, Numer. Math. 123 (2013) 363–393.

[34] S. Zampini, Dual-primal methods for the cardiac bidomain model, Math. Mod. Meth. Appl. Sci. 24 (4) (2014) 667–696.

[35] J. H. Bramble, J. E. Pasciak, J. Xu, Parallel multilevel preconditioners, Math. Comp. 55 (191) (1990) 1–22.

[36] B. Aksoylu, M. Holst, S. Bond, Implementation and theoretical aspects of the bpx preconditioner in the three dimensional local mesh refinement setting, Tech. Rep. ICES-04/50, Institute for Computational Engineering and Sciences, The University of Texas at Austin, Austin, TX, 2004 (2004).

[37] B. Aksoylu, M. Holst, Optimality of multilevel preconditioners for local mesh refinement in three dimensions, SIAM J. Numer. Anal. 44 (3) (2006) 1005–1025.

[38] W. Dahmen, A. Kunoth, Multilevel preconditioning, Numer. Math. 63 (1992) 315–344.

[39] M. Bendahmane, R. Buerger, R. Ruiz-Baier, A multiresolution space-time adaptive scheme for the bidomain model in electrocardiology, Numer. Meth. Part. Diff. Eq. 26 (6) (2010) 1377–1404.

[40] P. Colli Franzone, P. Deuflhard, B. Erdmann, J. Lang, L. F. Pavarino, Adaptivity in space and time for reaction-diffusion systems in electrocardiology, SIAM J. Sci. Comput. 28 (3) (2006) 942–962.

[41] P. Deuflhard, B. Erdmann, R. Roitzsch, G. T. Lines, Adaptive finite element simulation of ventricular dynamics, Comput. Visual. Sci. 12 (2009) 201–205.

[42] J. Southern, J. G. J. Gorman, M. D. Piggot, P. E. Farrel, Parallel anisotropic mesh adaptivity with dynamic load balancing for cardiac electrophysiology, J. Comput. Sci. 3 (1-2) (2012) 8–16.

[43] J. Southern, J. G. J. Gorman, M. D. Piggot, P. E. Farrel, M. O. Bernabeu, J. Pitt-Francis, Simulating cardiac electrophysiology using anisotropic mesh adaptivity, J. Comput. Sci. 1 (2) (2010) 82–88.

[44] J. A. Trangestein, C. Kim, Operator splitting and adaptive mesh refinement for the luo-rudy i model, J. Comput. Phys. 196 (2004) 645–679.

[45] J. P. Whiteley, Physiology driven adaptivity for the numerical solution of the bidomain equations, Ann. Biomed. Engrg. 35 (9) (2007) 1510–1520.

[46] D. Zipes, J. Jalife, Cardiac Electrophysiology: From Cell to Bedside, W. B. Saunders Co., 6th ed., Philadelphia, 2013.

[47] J. P. Keener, J. Sneyd, Mathematical Physiology, Springer, 1998.

[48] M. Pennacchio, G. Savaré, P. Colli Franzone, Multiscale modeling for the bioelectric activity of the heart, SIAM J. Math. Anal. 37 (2006) 1333–1370.

[49] L. Tung, A bi-domain model for describing ischemic myocardial d-c potentials, PhD Thesis, MIT, Cambridge, MA (1978).

[50] C. S. Henriquez, Simulating the electrical behavior of cardiac tissue using the bidomain model, Crit. Rev. Biomed. Engrg. 21 (1993) 1–77.

[51] C. Luo, Y. Rudy, A model of the ventricular cardiac action potential: depolarization, repolarization, and their interaction, Circ. Res. 68 (1991) 1501–1526.

[52] Y. Bourgault, Y. Coudiere, C. Pierre, Existence and uniqueness of the solution for the bidomain model used in cardiac electrophysiology, Nonlin. Anal. Real World Appl. 10 (1) (2009) 458–482.

[53] M. Veneroni, Reaction-diffusion systems for the macroscopic bidomain model of the cardiac electric field, Nonlin. Anal. Real World Appl. 10 (2) (2009) 849–868.

[54] J. Maes, A. Kunoth, A. Bultheel, Bpx-type preconditioners for 2nd and 4th order elliptic problems on the sphere, SIAM J. Numer. Anal. 45 (1) (2007) 206–222.

[55] A. Buffa, H. Harbrecht, A. Kunoth, G. Sangalli, BPX-preconditioning for isogeometric analysis, Comput. Meth. Appl. Mech. Engrg. 265 (2013) 63–70.

[56] Y. Saad, Iterative methods for sparse linear systems, SIAM, Philadelphia, 2003.

[57] S. Balay, S. Abhyankar, M. F. Adams, J. Brown, P. Brune, K. Buschelman, V. Eijkhout, W. D. Gropp, D. Kaushik, M. G. Knepley, L. C. McInnes, K. Rupp, B. F. Smith, H. Zhang, PETSc Web page, `http://www.mcs.anl.gov/petsc` (2014).
URL `http://www.mcs.anl.gov/petsc`

[58] S. Balay, S. Abhyankar, M. F. Adams, J. Brown, P. Brune, K. Buschelman, V. Eijkhout, W. D. Gropp, D. Kaushik, M. G. Knepley, L. C. McInnes, K. Rupp, B. F. Smith, H. Zhang, PETSc users manual, Tech. Rep. ANL-95/11 - Revision 3.5, Argonne National Laboratory (2014).
URL `http://www.mcs.anl.gov/petsc`

[59] [link].
URL `http://cluster.mat.unimi.it`

[60] A. Xu, M. R. Guevara, Two forms of spiral-wave reentry in an ionic model of ischemic ventricular myocardium, Chaos 8 (1) (1998) 157–174.

[61] K. H. W. J. ten Tusscher, D. Noble, P. J. Noble, A. V. Panfilov, A model for human ventricular tissue, Am. J. Phys. Heart. Circ. Physiol. 286 (2004) H1573–H1589.

[62] T. R. Shannon, F. Wang, J. Puglisi, C. Weber, D. M. Bers, A mathematical treatment of integrated ca dynamics within the ventricular myocyte, Biophys. J. 87 (5) (2004) 3351–3371.

[63] V. E. Henson, U. M. Yang, BoomerAMG: A parallel algebraic multigrid solver and preconditioner, Appl. Numer. Math. 41 (2002) 155–177.

[64] [link].
URL `http://acts.nersc.gov/hypre`

[65] A. Hodgkin, A. Huxley, A quantitative description of membrane current and its application to conduction and excitation in nerve, J. Physiol. (London) 117 (1952) 500–544.

[66] Y. Rudy, J. R. Silva, Computational biology in the study of cardiac ion channels and cell electrophysiology, Quart. Rev. Biophys. 39 (1) (2006) 57–116.

[67] P. Colli Franzone, L. F. Pavarino, S. Scacchi, Mathematical Cardiac Electrophysiology, Springer, New York, 2014.